Journal of Hazardous Materials 161 (2009) 824–834

Contents lists available at ScienceDirect

Journal of Hazardous Materials

journal homepage: www.elsevier.com/locate/jhazmat

Adsorption behavior of Zn(II) on calcinated Chinese loess

Xiaowu Tang*, Zhenze Li, Yunmin Chen

MOE Key Laboratory of Soft Soils and Geoenvironmental Engineering, Department of Civil Engineering, Zhejiang University, Zheda Road 38, Hangzhou 310027, PR China

ARTICLE INFO

Article history:
Received 24 August 2007
Received in revised form 9 April 2008
Accepted 9 April 2008
Available online 22 April 2008

Keywords:
Adsorption
Zn(II)
Loess
Calcination
Kinetics

ABSTRACT

Chinese loess has proven to be effective in removing Zn(II) from aqueous solutions, but the resultant adsorbent–water slurry is difficult to separate. In this paper, the crude loess was calcinated to improve the separation efficiency of slurries in terms of sedimentary rate by increasing the particle sizes of the adsorbent. The sorption capacities of different sorbents, including crude loess, calcinated loess, de-organic crude loess and acid-treated calcinated loess, were obtained and sequenced. The adsorption capacity of the calcinated loess towards Zn(II) was found to be as high as 113.6 mg g^{-1}. The adsorption isotherms and kinetics of calcinated loess were best-fit with the Freundlich isotherm and the pseudo-second order kinetics, respectively. The thermodynamic analysis revealed that the adsorption was exothermic and spontaneous with a high preference for Zn(II) removal. The adsorption of Zn(II) on calcinated loess implies an ion exchange of the solute with calcite and goethite due to the observed FT-IR and XRD patterns as well as the predicted mean free energies (−11.58 to −9.28 kJ mol^{-1} by D–R model). The byproduct of adsorption can be purified and refreshed by using a 0.01 M HCl solution.

1. Introduction

Zinc is one of the main pollutants in acid mining drainages. In developing countries, metal mining and metallurgy industrial departments produce large quantities of wastewater containing high concentration of Zn(II) [1,2]. Considering the toxicity of Zn(II), treatment methods have been widely developed. Chemical precipitation is the most widely adopted method. Due to the low dissolution coefficient of zinc sulfide, sodium sulfide or hydrogen sulfide is always used to remove ionic zinc from aqueous solution to extremely low or nondetectable levels [3,4]. Chemical precipitation can also be obtained by adjusting the solution pH to alkaline states which will lead to the precipitation of Zn(II) [5]. Nevertheless, the costs of chemical additives are high and the salinity of the wastewater will be increased, which limits the applicability of this method.

Fixation of Zn(II) through ion exchange is also an optional treatment method. A selective elimination is possible by means of heavy metal-selective ion exchangers which exhibit a high affinity for heavy metals. However, this method is not extensively adapted to metals removal in industrial wastewater treatment [6].

Adsorption can be used to attain a similar target. Many sorbents have been developed and are being continually tested. Minerals such as apatite and goethite have been reported with excellent purifying capabilities for metal cations. Industrial wastes such as activated sludge, coal fly ash and iron slag have also been studied for the applicability for Zn(II) removal. Natural products such as leaf [7], coca shell [8] and sea weed [9], can be used to remove heavy metals by producing activated carbons through further processing. Several kinds of natural soils have been observed to have high adsorption capacity for Zn(II) and optimum conditions have also been extensively investigated and reported [10–12].

Chinese loess is widely distributed throughout western China and has been studied as an adsorbent for Zn(II) removals from aqueous solution in the authors laboratory. The intrinsically abundant constituent in loess is calcite. Calcite has been found to play a major role in Zn(II) adsorption [13,14]. The adsorption capacity is rather high in comparison with other adsorbents, showing potential utilizability in practice. In western China, the acid mining drainage is a major source of contamination to the environment. It is particularly beneficial to investigate the applicability of locally prolific loess for wastewater treatment. Since the main composition of loess is clay and silt [15], the treatment of Zn(II) in solution produces mixtures with a large amount of fine solids that are difficult to filter or precipitate. The separation of the sorbent after equilibrating with Zn(II) solution becomes an intractable engineering problem.

The main objectives of this paper are to develop a method to improve the separating properties of loess after adsorption with Zn(II) and to investigate the adsorbing behavior as well as the intrinsic uptake mechanism. Firstly, the improvement of the sedimentary rate of the adsorbent requires an increased particle size of the sorbent that could be achieved after calcination at moder-

* Corresponding author. Tel.: +86 571 87951714; fax: +86 571 85023966.
E-mail address: tangxiaowu@zju.edu.cn (X. Tang).

0304-3894/$ – see front matter © 2008 Elsevier B.V. All rights reserved.
doi:10.1016/j.jhazmat.2008.04.059

ately high temperatures. Secondly, the Zn(II) adsorption behavior of the obtained sorbent was investigated and compared with those of the crude loess without any treatment. Finally, several factors, including solution pH, slurry concentration, reaction duration and temperature, which may affect the adsorption behavior of Zn(II) on the sorbent, were studied. The treatment method for the sorbent adsorbed with Zn(II) was also studied for possible recycling utilization.

2. Materials and methods

2.1. Preparation of the adsorbent

Crude loess (CL) was taken from suburban area of Xi'an, China. The soil was put into a clean ceramic cup and oven calcinated at 650 °C for 7 h [16]. The calcinated loess (CAL) was ground to a powder with a ceramic mortar and then stored in a plastic bag after being cooled down to room temperature. The mortar was previously cleaned three times with deionized water (DW) and then polished with ethanol to avoid contamination of the samples. The crude soil and the acid-treated calcinated soil (ATCAL) were also utilized in the study of the adsorption mechanism. The ATCAL was prepared by mixing the CAL with 0.1 M HCl solution and equilibrated for 24 h under continuous whisking. The residual solid was separated from the mixture by passing the slurry through a 0.45 μm PE filter membrane. The crude soil was further purified by removing the natural organics with H_2O_2 solution.

2.2. Characterization of the sorbent

The distributions of grain size for both the crude and calcinated loess were determined. Particles larger than 0.075 mm were tested using a series of sieves while the remaining soil was tested using the sedimentary method. The organic content of both soils was measured by the weight loss after igniting the soil at 650 °C for 8 h in the presence of oxygen. The cation exchange capacity (CEC) of both soils was tested using the ammonium exchange method. The specific surface area was determined using the N_2 adsorption method and the results were analyzed with the BET adsorption theory. The natural pH of soil was determined by measuring the pH of slurry (0.1 g/50 mL) equilibrated for 24 h using a glass potentiometer.

TEM, FT-IR and XRD spectra of both the crude and the calcinated loess were conducted. The adsorbent sample was transferred into the deionized water and stirred vigorously for 10 min. The mixture was then left static for 24 h. The supernatant was sampled and spotted onto a clean copper net for the Transmittance Electronic Microscopy (TEM) test by JEOL 200CX (JEOL, Japan). The sample was dissolved in water for this test rather than in ethanol which is the standard procedure of TEM test. The evaporation of the sample on the copper net took much longer than that required following the common testing procedure.

XRD patterns of the sorbents (i.e., crude loess, calcinated loess and Zn(II) saturated loess), were carried out on D/MAX-RA apparatus (Rigaku Corporation, Japan) with a rotating anode Cu Kα. Dried samples with CL, CAL, ATCAL and Zn(II) saturated calcinated loess were separately ground with KBr into fine powders under infrared radiation before slices were produced by compression under 40 MPa. The FT-IR pattern for each sample was then recorded on the Nexus-670 (Nicolet, USA).

2.3. Methods

The sedimentary rates of the prepared adsorbents, the adsorption isotherms, the adsorption behaviors under different pH, temperature, slurry concentration and equilibrium time and the recycling method of the used adsorbent were shown as follows.

2.3.1. Test of sedimentary rate

The sorbent (0.500 ± 0.002 g) was measured and mixed with 250 mL DW. The mixture was equilibrated under consistent stirring for 24 h and then placed in a graduated flask. The sorbent–water mixture was sampled (3.0 mL) at the midpoint (i.e., vertical direction) of the liquid in the flask. The concentrations of soil particles and colloid particles are related to the transmittance of the mixture. The photospectrometry (UV-1800, China) was used to determine the slurry concentration qualitatively with DW used for comparison. The wavelength was chosen as 650 nm in this test.

2.3.2. Effect of pH

The CAL (0.100 ± 0.002 g) and the $ZnSO_4$ solution (200 mg L^{-1}, 50 mL) were transferred to a flask. The initial pH (pH_0) of the solution was increased from 1.5 to 6.8 by adding 0.1 M HCl or NaOH solution. The volume of the additive was not allowed to surpass 5% of the total volume of the solution. The sample bottles were put in a rotating box at 180 rpm for 24 h. The temperature was regulated at 25 °C with a prefabricated air conditioner. The solution pH was measured by glass electrode at the end of the test (pH 213, China). The solution was placed in PVC bottles for centrifugation at 3000 rpm for 5 min. The supernatant was sampled to determine the Zn(II) concentration using the Atomic Absorption Spectroscopy (AAS) method with the Hitachi 180-80 apparatus (Japan). Control and parallel tests were conducted and the results were averaged.

2.3.3. Adsorption kinetics

The slurry concentration was fixed as 0.1 ± 0.002 g/50 mL while the initial Zn(II) concentration (C_0) varied from 50 to 200 mg L^{-1} in increments of 50 mg L^{-1}. Batch adsorption was carried out under a constant temperature 25 °C while rotating at 180 rpm. In order to measure the solute concentration at certain times after the equilibration reaction was started, the sample bottle was taken out of the agitator and left stand for 3 min before 50 mL solution was sampled from the supernatant. The sampled solution, which contained solid phase, was filtered through a 0.45 μm PE filter membrane. The filter was washed twice with DW to decrease the loss of solute and a clear solution was diluted for determination of the Zn(II) concentration. Sampling was repeated with increasing reaction durations up to 24 h. Control and parallel tests were conducted and the results were averaged.

2.3.4. Adsorption isotherms at different temperatures

The Zn(II) adsorption isotherms of CAL (0.1 ± 0.002 g/50 mL) were carried out using batch tests where the initial Zn(II) concentration ranged from 25 to 250 mg L^{-1}. Four sets of isothermal adsorption tests were conducted at 5, 15, 25 and 35 °C separately.

Table 1
Grain size distribution of crude and calcinated loess and related characteristics

	Sand % (>0.05 mm)	Silt % (0.05–0.005 mm)	Clay % (<0.005 mm)	Organic (mg g^{-1})	CEC (meq/100 g)	Natural pH	Specific surface area (m^2 g^{-1})
Loess	14.1	65.4	20.5	5.5	8.6	8.2	24.1
Calcinated loess	15.6	78.3	6.1	0.0	6.2	7.8	20.7

Each test was equilibrated for 24 h and the equilibrium Zn(II) concentration was determined using AAS method to calculate the adsorption amount on the sorbent. Controls and parallel tests were conducted and the results were averaged.

2.3.5. Effect of slurry concentration

The Zn(II) solution (50 mL, 200 mg L^{-1}) was measured and poured into a flask. Five pieces of the adsorbent CAL were weighted from 0.1 ± 0.002 to 0.5 ± 0.002 g with an increment of 0.1 g and filled into the sample bottles. The pH of the solution was not adjusted in this test. Other conditions including temperature 25 °C, rotating speed 180 rpm and equilibrium duration 24 h were modulated during the equilibration process, in a manner similar to that of the above tests. The equilibrium Zn(II) concentration was determined using the AAS method. Controls and parallel tests were conducted and the results were averaged.

2.3.6. Treatment of the byproduct

The sorbent (1 ± 0.02 g CAL) was weighted and saturated with 1 L Zn(II) (500 mg L^{-1}) solution for 24 h under consistent agitation. The solid fraction was separated by settling for 24 h and then oven-dried. A specified quantity of Zn(II) saturated sorbent was measured

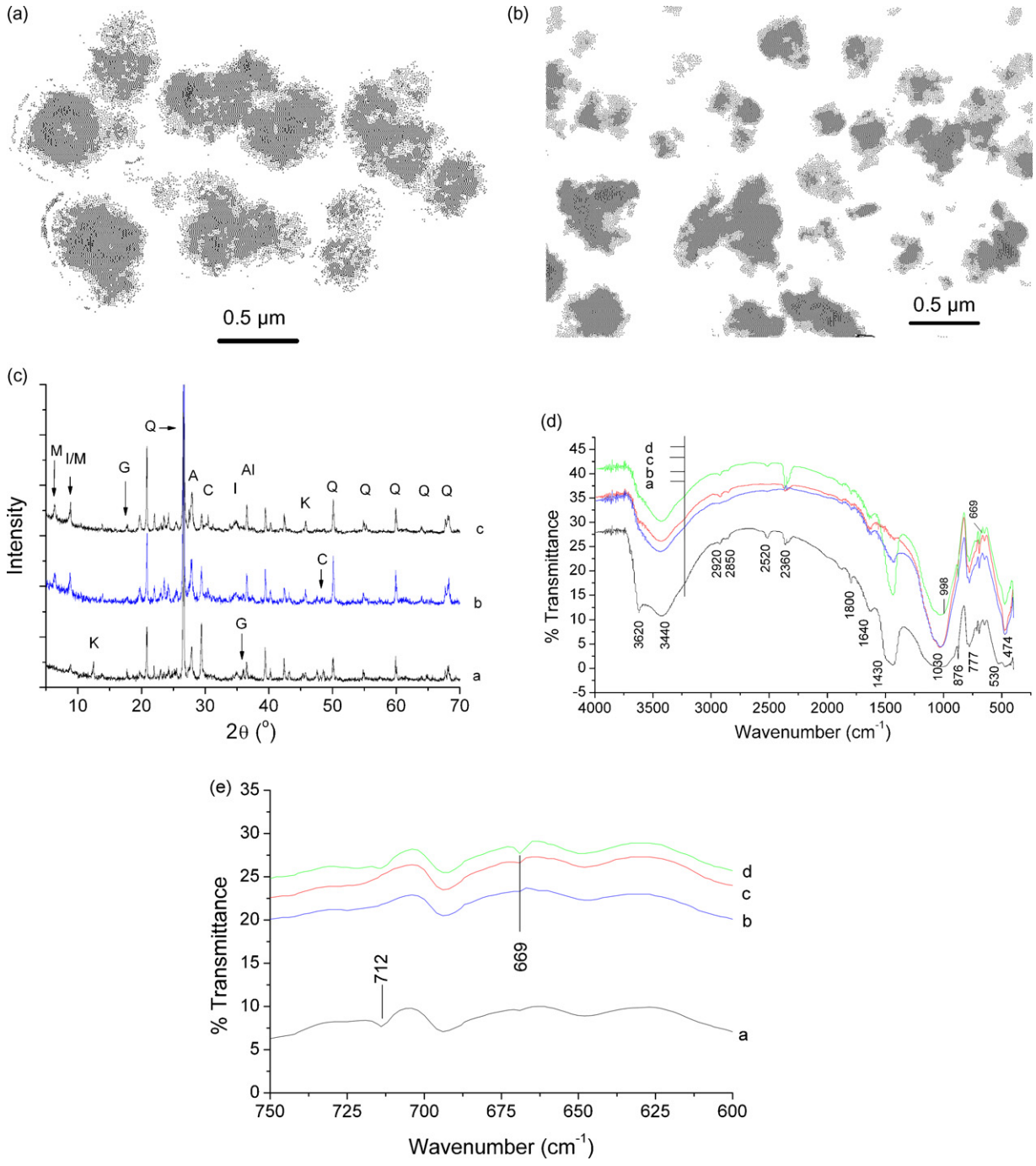

Fig. 1. (a) TEM photo of calcinated Chinese loess. (b) TEM photo of crude Chinese loess. (c) XR-D spectrum for sorbents (a: CL, b: CAL, c: Zn(II) loaded CAL) A: albite, Al: aluminum oxide, C: calcite, G: goethite, I: illite, K: kaolinite, M: muscovite, Q: quartz. (d) FT-IR patterns in the whole range of sorbents (a) CL, (b) Zn(II) loaded CAL, (c) ATCAL, (d) CAL. (e) FT-IR patterns in limited ranges of wavenumber for sorbents (a) CL, (b) Zn(II) loaded CAL, (c) ATCAL, (d) CAL.

and transferred into a bottle with 50 mL 0.01 M HCl. The mixture was shaken at 180 rpm on an agitator for 5 h. The obtained solution was centrifuged for 5 min at 3000 rpm. The supernatant was sampled to determine the equilibrium Zn(II) concentration. The residual Zn(II) concentration in the sediment was measured using the ICP method. Control and parallel tests were conducted and the results were averaged.

3. Results and discussions

3.1. Characterization of the sorbent

Table 1 shows the grain size distribution of the adsorbents. The clay component decreases from 20.5% of CL to 6.1% of the CAL. After calcination, the mass percentages of sand and silt particles increase from 14.1 and 65.4 in CL to 15.6 and 78.3 in CAL, respectively. And the specific surface area of the adsorbents is found to decrease from 24.1 to 20.7 $m^2\,g^{-1}$. It is obvious that the particle sizes are greatly increased by the calcination of CL. Other basic physicochemical parameters, including the organic content, the CEC and the natural pH, are determined as 5.5%, 8.6 meq/100 g and 8.2, respectively, for crude loess. For calcinated loess, these parameters are 0%, 6.2 meq/100 g and 7.8, respectively.

Fig. 1(a) shows the transmission electron microscopic features of particles that have been glued together after calcination. This observation is in agreement with the decreased clay content and the SSA shown in Table 1. The sedimentary rate was significantly increased and this may help to separate the solid from the liquid phase. Fig. 1(b) shows the small and dispersive particles of crude loess with irregular shapes (e.g. sharp protuberances and deep pits on the surface). The volume of inner pores and adsorption capacity might be increased as shown in Fig. 1(a); however, the specific surface area of loess declined after calcination due to the cementation of soil particles.

XRD and FT-IR spectra of the adsorbents were also determined and the results are shown in Fig. 1(c–e). From Fig. 1(c), several clay minerals including kaolinite, illite, calcite, quartz, albite and goethite were observed in the CL. It has been reported that the clay mineral constituents of Quaternary Chinese loess, sampled from the similar sites to our study, showed illite (55–75%), kaolinite (10–25%) and mixed layer mineral (10–20%) [17]. The major clay minerals (illite and kaolinite) can be identified in Fig. 1(c).

Part of the kaolinite originally found in crude loess disappears after calcination while a new band occurred at 6.32 (2θ) corresponding to the presence of montmorillonite. The quantity of goethite is also found to decrease in the treated adsorbent. The decreased band strength corresponding to calcite indicates the possible decomposition of $CaCO_3$ at high temperature. The decomposition temperature of calcite is reported as 853 °C, about 200 °C higher than the calcination temperature selected in this study [16]. However, other minerals or chemicals found in crude loess (i.e., potassium salts or sodium salts), may contribute to this process and lead to the decay at lower temperature.

Because of the positive effect of carbonate on the uptake of heavy metal cations, it is necessary to preserve the original abundance for the purpose of maintaining a moderately high sorption capacity. The selected temperature for calcination is reasonable for improving the separation behavior of the sorbent in aqueous slurry, although a part of calcite did decompose in this study,

From the IR patterns shown in Fig. 1(d and e), the change of surface hydroxyl groups can be identified from the adsorption band at 3620 cm^{-1}. The absorption intensity of the band at 1430 cm^{-1} which is assigned to calcite does not undergo much change between spectra *a* and *d*. This mineral has been reported as an effective sorbent for heavy metals during precipitation [14]. The treatment of the CL does not appear to destruct the originally contained calcite and thus the adsorption capacity of the CL is fully preserved in the CAL.

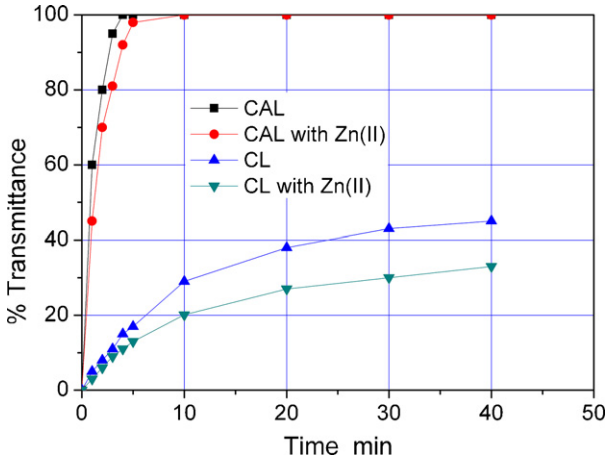

Fig. 2. Variation of transmittance of sorbent slurries with settling time.

3.2. Sedimentary rate of the sorbent

The sedimentary rate of calcinated loess was greatly improved compared to that of crude loess according to Fig. 2. The time at which the transmittance of CAL can reach 100% was determined to be 4 min, but increased to 6 min after saturated with Zn(II). Contrarily, the transmittance of the CL reached a plateau of 40% within 40 min, and even decreased to 31.5% after saturated with Zn(II). The presence of citric acid was reported to result in a stable suspension of alumina particles in the slurry [18]. The higher percentage of clay minerals and natural organics in CL could lead to a lower sedimentation rate. The adsorption of Zn(II) may worsen this phenomenon by causing the alteration of the surface functional groups and surface charges that weaken the interactions (i.e., H-bonds and oriented bonds by electrostatic effects, between soil particles). Therefore, the calcination of loess is effective in enhancing the separation efficiency of the sorbent from the liquid at the end of wastewater treatment.

3.3. Effect of pH

Fig. 3 shows the effect of pH_0 on Zn(II) adsorption on CAL. The equilibrium adsorption amount (q_e) was strongly affected by solution pH. The q_e is less than 10 mg g^{-1} at $pH_0 < 3.0$ and increases accordingly with a further increase in pH_0 and finally reach a maximum value at pH_0 equal to 6.8.

The equilibrium pH (pH_e) in solution was also determined and shown in Fig. 3. The superior buffering effect of loess can be recognized with respect to the increased pH_e compared to the pH_0. The maximum pH_e was observed as 7.25 at pH_0 4.2, while the further increase of pH_0 resulted in declined pH_e. However, the pH_e values of the sorbent–solution mixture were all less than that of the natural soil (pH_{na} 8.72). This may be caused by an ion exchange type adsorption of Zn(II) on CAL that releases hydrogen ions and leads to the decrease of pH_e.

3.4. Effect of slurry concentration

Fig. 4 shows that the amount of adsorbed Zn(II) on loess decreased with increasing slurry concentration from 0.1 to

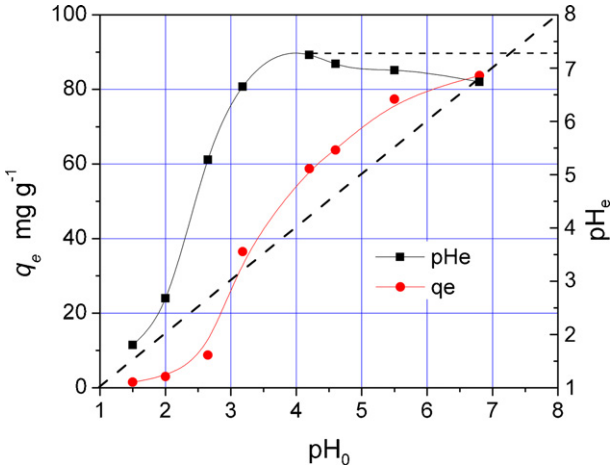

Fig. 3. Variation of Zn(II) adsorption amount on CAL with varied initial pHs.

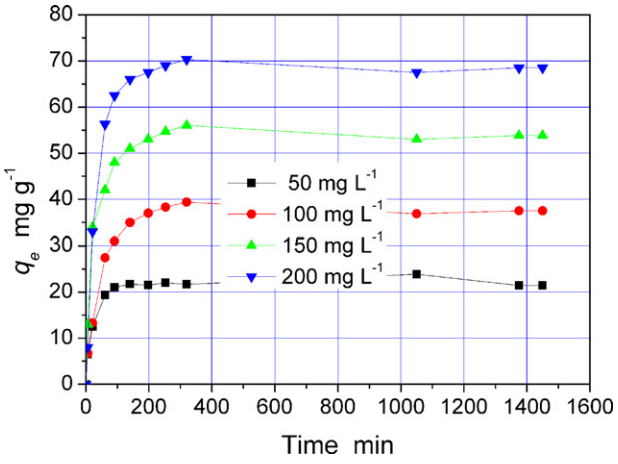

Fig. 5. Test data of adsorption kinetics (25 °C, 0.100 g/50 mL).

0.5 g/50 mL. For solutions with fixed initial solute concentrations, the removal percentage of Zn(II) increased with increasing slurry concentration but the unit adsorption quantity decreased at the expense of the efficiency of the process. A similar phenomenon was observed in solute adsorption on the crude loess. It is reported that the hydrolysis radius of soil particles become less at high sorbent concentrations due to chemical interactions (e.g. flocculation and the overlap of the hydrolysis layers between colloid particles) [19]. The effective contact surface area of the sorbent with the solution declines, resulting in a decreased unit sorption capacity.

3.5. Adsorption kinetics

Fig. 5 shows the variation of q_e of Zn(II) on CAL with increasing equilibration durations. The time required to reach the adsorption equilibrium increased from 91 to 320 min with an increasing initial solute concentrations from 50 to 200 mg L^{-1}. The test data were further analyzed with three kinetic models (i.e., pseudo-first order kinetics, pseudo-second order kinetics and intraparticle diffusion model).

The pseudo-first order kinetic equation is [20]:

$$\lg(q_e - q_t) = \lg(q_e) - \frac{k_1}{2.303}t \quad (1)$$

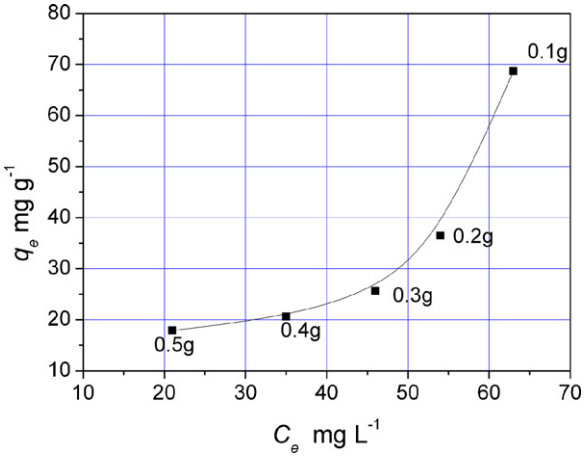

Fig. 4. Effect of slurry concentrations on Zn(II) adsorption amount of CAL (unadjusted pH, 25 °C, C_0 = 200 mg L^{-1}).

where q_e and q_t are the amount of solute adsorbed per unit adsorbent at equilibrium and any time, respectively (mg g^{-1}), and k_1 the pseudo-first order rate constant (min^{-1}).

The pseudo-second order kinetic equation is [20]:

$$\frac{t}{q_t} = \frac{1}{k_2 q_e^2} + \frac{1}{q_e}t \quad (2)$$

where k_2 is the pseudo-second order rate constant (g mg^{-1} min^{-1}).

The equation on the intraparticle diffusion model is [21]:

$$q_t = k_{int}t^{1/2} + C \quad (3)$$

where k_{int} is the relevant rate constant (mg g^{-1} min$^{-1/2}$) and C is the intercept.

Table 2 shows the predicted model constants for the above kinetic equations. The pseudo-second order kinetic equation was found to best-fit the test data as judged by the correlation coefficients. The linear fit of the test data with the pseudo-first order kinetic equation is shown in Fig. 6 and agreed well within the beginning 325 min but later became unreasonable. (*Note*: data were not presented in the figure.) The equilibrium adsorption amounts predicted by the pseudo-second order kinetic equation are close to those observed in Fig. 7. The rate constant k_2 was found decreased from 10.87 to 1.32, 1.95 and 0.86 × 10^{-3} g mg^{-1} min^{-1} with increasing C_0 from 50 to 100, 150 and 200 mg L^{-1}, respectively. It is shown that the solution with diluted Zn(II) concentration is easy to equilibrate by the CAL.

Table 2
Predicted kinetic constants for Zn(II) adsorption on CAL

	C_0 (mg L^{-1})			
	50	100	150	200
Pseudo-first order kinetics				
q_e (mg g^{-1})	14.10	39.82	41.89	61.54
k_1 (×10^{-3} min^{-1})	20.61	16.81	15.59	22.98
R^2	0.953	0.966	0.967	0.997
Pseudo-second order kinetics				
q_e (mg g^{-1})	21.98	38.02	54.11	69.30
k_2 (×10^{-3} g mg^{-1} min^{-1})	10.87	1.32	1.95	0.86
R^2	0.997	0.999	1.000	0.999
Intraparticle diffusion model				
k_{i1} (mg g^{-1} min$^{-1/2}$)	2.25	3.25	5.08	7.11
C_1	0.90	−0.59	2.61	−2.72
R_1^2	0.992	0.992	0.973	0.987
k_{i2} (mg g^{-1} min$^{-1/2}$)	–	1.27	1.29	1.28
C_2	–	17.35	33.71	48.14
R_2^2	–	0.995	0.968	0.964

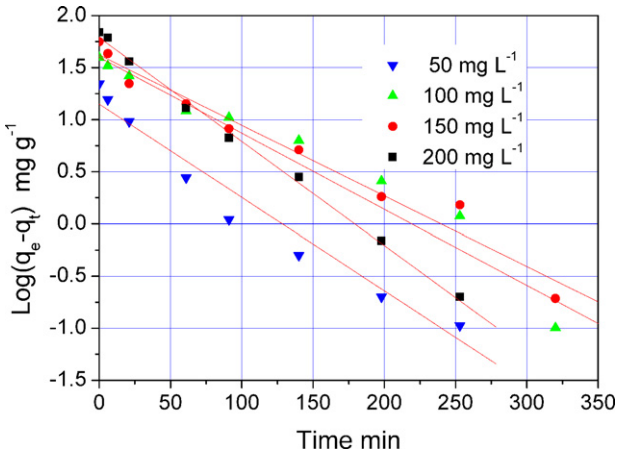

Fig. 6. Linear fit of kinetic test data with pseudo-first order kinetics.

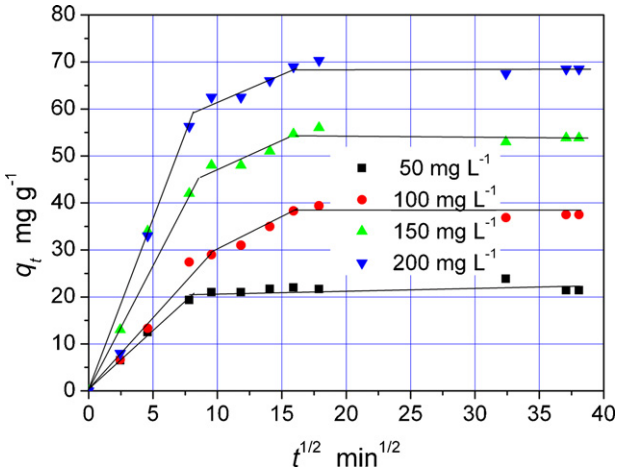

Fig. 8. Linear fit of kinetic test data with intraparticle diffusion model.

The intraparticle diffusion model considers the sorption as a three-stage process: the rapid adsorption, the gradual inward diffusion and the final equilibration. Fig. 8 shows the multilinearity of simulated curves for the test data which confirms these assumptions. The adsorption process can be divided into three stages for solutions with initial concentrations, C_0 = 100, 150 and 200 mg L^{-1}. However, the absence of the second linear portion was observed in solution with C_0 = 50 mg L^{-1}, indicating that the sorption was mainly surface adsorption. The rate constant k_{i1}, predicted by the intraparticle model was found to increase from 2.25 to 3.25, 5.08 and 7.11 mg g^{-1} $min^{-1/2}$ as C_0 increased from 50 to 100, 150 and 200 mg L^{-1}, respectively. Nevertheless, the rate constant k_{i2} remained steady as 1.27–1.29 mg g^{-1} $min^{-1/2}$ at higher solute concentrations such as 100, 150 and 200 mg L^{-1}, indicating that the diffusion of Zn(II) was not affected by solute concentrations and thus may be the rate limiting stage. Since there was no obvious change of the rate (k_{i2}) of diffusion in the diverse solute concentrations, the adsorption of Zn(II) in this stage may not impose a significant influence on the microstructures (e.g. pore blocks or destructions).

Based on the above discussions, the adsorption of Zn(II) on CAL can be considered wholly as the surface adsorption at low Zn(II) concentration (50 mg L^{-1}), and as the combination of surface adsorption and pore-filling by diffusing at higher Zn(II) concentrations (100, 150 and 200 mg L^{-1}).

3.6. Adsorption isotherms and effect of temperature

Fig. 9 shows the adsorption isotherms of Zn(II) on CAL at different temperatures. Three isothermal equations were applied to evaluate the test results.

The Langmuir isotherm can be written as [20]:

$$\frac{C_e}{q_e} = \frac{1}{bQ} + \frac{C_e}{Q} \quad (4)$$

where C_e is the equilibrium concentration of solute solution (mg L^{-1}), Q the maximum surface density of adsorbent (L mg^{-1}) and b is the Langmuir constant.

The Freundlich isotherm can be expressed as [20]:

$$q_e = K_F C_e^{1/n} \quad (5)$$

where K_F is the Freundlich constant (mg g^{-1}) indicating the adsorption capacity and strength of the adsorptive bond and n is the heterogenity factor.

Dubinin–Radushkevich (D–R) isotherm is based on the concept of energy and can be written as [20]:

$$\ln q_e = \ln q_m - k\varepsilon^2 \quad (6)$$

where q_m is the maximum adsorption capacity (mol g^{-1}), and k is the constant related to the adsorption energy.

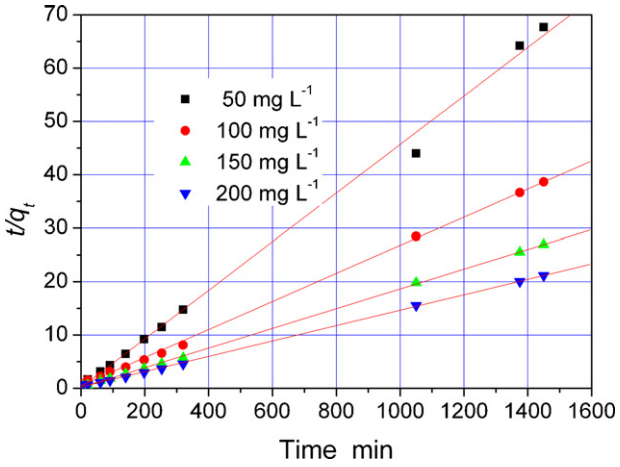

Fig. 7. Linear fit of kinetic test data with pseudo-second order kinetics.

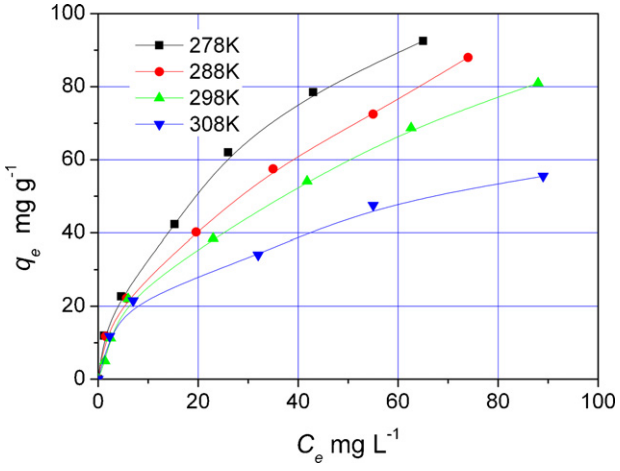

Fig. 9. Isotherms of Zn(II) adsorption on CAL.

Table 3
Predicted isothermal constants for Zn(II) adsorption on CAL

	278 K	288 K	298 K	308 K
Langmuir model				
Q (mg g^{-1})	113.636	105.932	98.717	62.344
b (L g^{-1})	0.054	0.044	0.038	0.064
R^2	0.954	0.929	0.959	0.965
Freundlich model				
K_F (mg g^{-1})	10.542	9.236	5.550	8.757
n	1.899	1.946	1.624	2.422
R^2	0.997	0.998	0.970	0.988
D–R model				
q_m (mg g^{-1})	363.439	307.201	389.021	156.243
k (mol^2 kJ^{-2})	0.0055	0.00511	0.00581	0.00373
E (kJ mol^{-1})	−9.53	−9.89	−9.28	−11.58
R^2	0.991	0.989	0.982	0.989

The Polanyi potential (kJ mol^{-1}) ε is written as:

$$\varepsilon = RT \ln\left(1 + \left(\frac{1}{C_e}\right)\right) \quad (7)$$

where the unit of C_e should be translated into mol L^{-1}.

The mean free energy of the adsorption E is

$$E = -\frac{1}{\sqrt{2k}} \quad (8)$$

The adsorption is basically a surface adsorption associated with ion exchange when $|E|$ is between 8 and 16 kJ mol^{-1} [20]. Otherwise, for $|E|$ ranging from 1.0 to 8.0 kJ mol^{-1}, the mechanism is physical adsorption [22].

Table 3 lists the predicted isothermal constants for Zn(II) adsorption on CAL based on the linearization of test data as shown in Figs. 10–12. Based on the correlating coefficients, the Freundlich model was found to fit the test data better than the Langmuir and D–R models. From the analysis of Langmuir isotherm, the maximum adsorption capacities of CAL were obtained at 113.6, 105.9, 98.7 and 62.3 mg g^{-1} at increased temperatures from 278 to 308 K with an increment of 10 K, respectively. The increase in temperature leads to the decline of adsorption capacity. As indicated by D–R isotherm analysis, the adsorption energy (E) increased from −11.58 to −9.53 kJ mol^{-1} with increasing temperature from 278 to 308 K, implying that the uptake of Zn(II) on CAL was mainly an ion exchange adsorption [20].

Table 4 shows the sorption capacity of different adsorbent. The equilibrium adsorption amount of CL was found to be as high as 216.0 mg g^{-1}, about twice that of the CAL. However, the sorption capacity of the CL decreases to 70.2 mg g^{-1} after the natural organics are removed. The ATCAL shows the least q_e as 15.9 mg g^{-1}. The sequence of the adsorption capacities for these sorbents is

$$\text{CL} > \text{CAL} > \text{DCL} > \text{ATCAL} \quad (9)$$

The natural organics, especially the microorganisms contained in CL will propagate under proper conditions and can greatly improve the adsorption capacity for heavy metals [7,22]. By comparing the CL and DCL, the contribution of the organics to q_e is equal to 145.8 mg g^{-1}. Such high sorption capacity makes CL an alternative for Zn(II) removal from an aqueous solution. However, the sorbent–solution mixture containing organics was difficult to separate from each other, as shown in Fig. 2. This limits the applicability of the CL to wastewater treatment. Although CAL has a comparatively lower sorption capacity than CL, it shows superior sedimentary behavior. The calcinated sorbent improves the shortage of the natural loess and exhibits possibilities in industrial utilization.

The Zn(II) adsorption behavior of ATCAL was also studied to evaluate the possibility of recycling the adsorbent by acid wash with hydrochloride. Fig. 13 shows the "H" type isotherm at 25 °C [23]. The relevant adsorption capacity of Zn(II) was determined as 15.9 mg g^{-1} as shown in Table 5 which was the lowest of all the adsorbents in this study. However, a high affinity towards Zn(II)

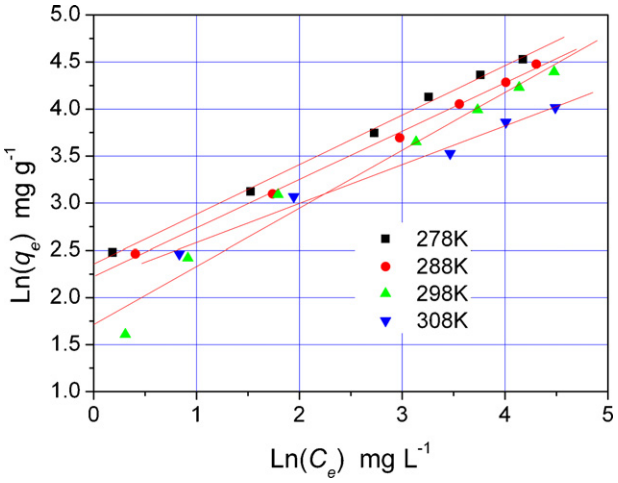

Fig. 11. Linear fit of adsorption isotherms with Freundlich model.

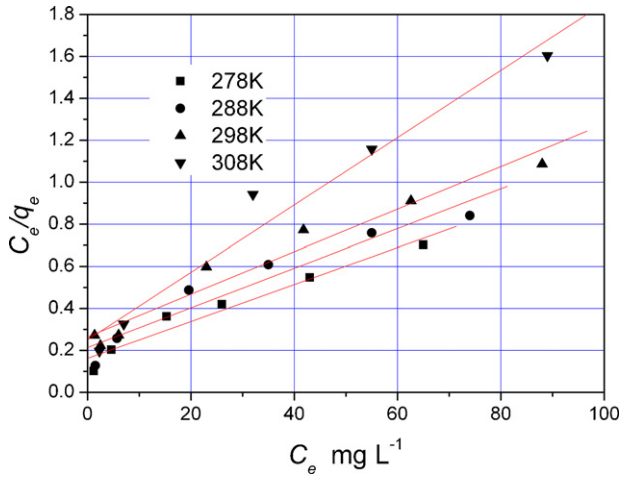

Fig. 10. Linear fit of adsorption isotherms with Langmuir model.

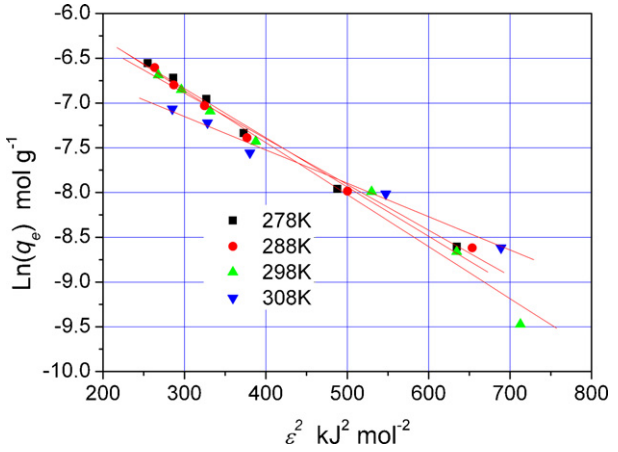

Fig. 12. Linear fit of adsorption isotherms with D–R model.

Table 4
Comparison of Zn(II) adsorption capacities on CL and treated loess

Sorbents	Crude loess (CL)	Calcinated loess (CAL)	De-organic crude loess (DCL)	Acid-treated calcinated loess (ATCAL)
q_e (mg g^{-1})	216.0	113.6	70.2	15.9

Data were obtained at 25 °C with the same slurry concentration and the solution pH was not adjusted in this study.

Table 5
Predicted isothermal constants for Zn(II) adsorption on ATCAL

Langmuir model			Freundlich			D–R			
Q (mg g^{-1})	b (L g^{-1})	R^2	K_F (mg g^{-1})	n	R^2	q_m (mg g^{-1})	k (mol^2 kJ^{-2})	E (kJ mol^{-1})	R^2
15.890	0.950	0.982	10.720	11.211	0.947	20.540	9.270E-04	−23.224	0.976

can still be identified. The test data were fitted with the Langmuir, Freundlich and D–R models and the simulated constants are listed in Table 5. The Langmuir model was found to be the best in fitting the isotherms. The free adsorption energy calculated by the D–R model was −23.224 kJ mol^{-1}. This implies a typical chemisorption with a strong bond between the ATCAL and Zn(II). The conditions for ion exchange do not exist any more since the surface hydroxyl group in kaolinite and montmorillonite has been greatly eliminated by calcinations. Other components of CAL (e.g. calcite and goethite), are dissolved by HCl treatment. Therefore, the adsorption of Zn(II) on such sorbent can be attributed mainly to stable minerals such as montmorillonite and kaolinite.

3.7. Thermodynamics

The thermodynamic behavior of Zn(II) adsorption on CAL was evaluated with the following equations:

$$\Delta G^0 = -RT \ln K_c \quad (10)$$

$$\Delta G^0 = \Delta H^0 - T\Delta S^0 \quad (11)$$

where K_c is the distribution coefficient of solute between adsorbent and solution in equilibrium (q_e/C_e), R the ideal gas constant, T the temperature (K), ΔH^0 the change of enthalpy, ΔS^0 the change of entropy and ΔG^0 is the standard Gibb's free energy. Eqs. (10) and (11) can be further written in form of linearized relationship between K_c and $1/T$ as:

$$\ln(K_c) = \frac{\Delta S}{R} - \frac{\Delta H}{RT} \quad (12)$$

The constants of thermodynamics as shown in Table 6 (i.e., the change of enthalpy (ΔH^0) and entropy (ΔS^0)), can be determined from the slope and intercept of the linearization of the test data as shown in Fig. 14.

The calculated enthalpy change and entropy change were −24.11 and −23.95 kJ mol^{-1}, respectively, implying an exothermic adsorption and a decreased freedom of the system. Positive entropy changes have been commonly reported and mainly attributed to the ion exchange with surface OH groups [7–9]. The adsorption sites have been greatly eliminated in CAL as shown in Fig. 1(c), and the ion exchange between Zn(II) and OH cannot be dominant in this system. This may constrain the entropy change toward positive values. On the other hand, the SO_4^{2-} in solution can react with Ca^{2+} and precipitate as $CaSO_4$ with low dissolving coefficients. This may decrease the ionic strength of the solution consequently. The negative entropy change also indicates the preferential uptake of Zn(II) on CAL. The predicted Gibbs free energy change ranged from −17.46 to −16.74 kJ mol^{-1} within the temperature ranges from 278 to 308 K, suggesting a spontaneous adsorption process.

3.8. Adsorption mechanism

Fig. 1(c) shows the XRD patterns of CAL and Zn(II) loaded CAL and only the content of calcite in CAL is found to decrease significantly

Table 6
Predicted thermodynamic constants for Zn(II) adsorption on CAL

ΔH (kJ mol^{-1})	ΔS (J mol^{-1} K^{-1})	T (K)	ΔG (kJ mol^{-1})
−24.11	−23.95	308	−16.74
		298	−16.98
		288	−17.22
		278	−17.46

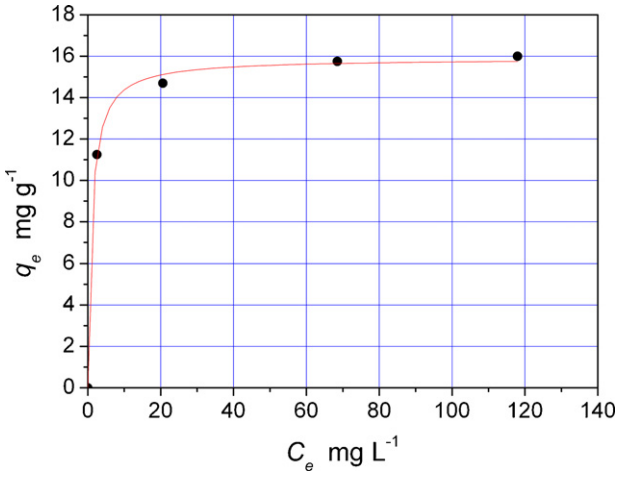

Fig. 13. Isotherm of Zn(II) adsorption on ATCAL (25 °C, 0.1 g/50 mL).

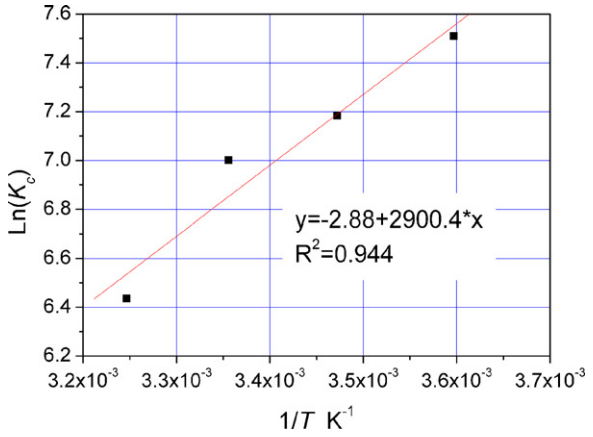

Fig. 14. Linear fit of thermodynamics for Zn(II) adsorption on CAL.

after being loaded with Zn(II). The species of the adsorbed Zn(II) on CAL cannot be identified in this figure. However, the reduction of calcite can be assigned to the ion exchange reaction with Zn(II) which can be written as:

$$Zn^{2+} + SO_4{}^{2-} + CaCO_3 \rightarrow ZnCO_3 + CaSO_4(\text{aqueous}) \quad (13)$$

Because the dissolving coefficient of calcium sulfate ($k_s = 10^{-4.61}$, data from database of MINTEQ A2 Ver. 4.0) is higher than those of $ZnCO_3$ ($k_s = 10^{-10.8}$) and $CaCO_3$ ($k_s = 10^{-8.48}$), the surface precipitate of gypsum may be limited and the micropores should not be blocked as a result. This is in agreement with the observation that there was no obvious change in the intraparticle diffusion rate k_{i2} at different C_0 due to the adsorption kinetic study. Since the dissolvability of the formation of $ZnCO_3$ is lower than that of calcite, the ion exchange process may take place mainly on the surface of the sorbent and break down before all the calcite is exhausted. Consequently, the Zn(II) saturated sorbent still contains a certain quantity of calcite as shown in XRD pattern of Zn(II) loaded CAL (i.e., line c in Fig. 1(c)).

The clay mineral of montmorillonite can be produced after the loess was calcinated at 650 °C for 7 h. Although the natural organics in CL have been eliminated, the newly formed montmorillonite helps to maintain the high adsorption capacity of CAL, corresponding to the sequence of Zn(II) adsorption capacity as shown in Eq. (9).

The FT-IR spectra are shown in Fig. 1(d and e) and are used to investigate the change of surface functional groups between CAL and Zn(II) loaded CAL. The bands at 694 and 777 cm^{-1} are assigned to quartz, an inert material showing little effect on Zn(II) adsorption. The bands at 712.68, 876, 1428.76, 1798.41 and 2513.52 cm^{-1} can be related to calcite. The content of calcite is significantly decreased after acid treatment and Zn(II) adsorption.

The band at 3620 cm^{-1} in CL, which is related to the surficial OH group, also decreases significantly after calcination. This functional group is known as an active adsorption site for heavy metals and is most likely to be attributed to natural organics and clay minerals [7–9]. As shown in Fig. 1(c), a certain quantity of clay minerals including illite and kaolin are contained in the crude loess. The adjacent OH groups on the surface of these minerals may react with each other to produce water molecules at high temperatures and thus lead to the cementation of adjacent soil particles by chemical bonds. Similarly, metasilicate have been reported produced in such a situation [16,24]. Table 1 shows that the decreased SSA of calcinated loess will inevitably reduce the available sorption sites for Zn(II) and may affect the adsorption capacity. However, the sorption capacity of CAL is still higher than that of DCL whose structure is similar to that of CL, indicating that the Zn(II) adsorption on loess may have several alternative mechanisms besides the surface complexation which is strongly linked to the surface OH group. The abundant micropores and chemicals in CAL may offset the loss of sorption capacity caused by the decrease of OH groups, which is verified by Zn(II) adsorption capacities.

The adsorption bands at 3440 and 1640 cm^{-1} can be assigned to the bending vibration of the sorbed water. No obvious changes in the intensities of such bands are observed in Fig. 1(d). Since the hydrolysis of KBr in air during the test can strongly influence the IR bands relevant to water molecules, the surface properties of the adsorbent cannot be distinctively identified regarding the adsorption behavior of water on loess.

The band at 536 cm^{-1} (corresponding to the group of Si–O–Al) in CL disappeared after calcinated by comparing spectra *a* and *d* in Fig. 1(d), implying the changes of silicate mineral compositions [24]. Sudo [16] has reported the similar evolution process of kaolinite in differential thermal analysis (DTA) and observed the loss of the OH group between silicon–oxygen tetrahedron and aluminium–oxygen octahedron at 535 °C. The conversion of kaolinite to montmorillonite has been confirmed by the XRD spectrum. Because the silicate tetrahedron is closely associated with the aluminium oxide hexahedron for kaolin but loosely for montmorillonite, the fingerprint IR band of the former (Si–O–Al) is much stronger than that of the latter. Once the mass percent of kaolinite is less than the detection limit, the relevant adsorption band will disappear.

The characteristic IR band of $ZnCO_3$ at 835.10 cm^{-1} was not detected in this study, differing from those reported by Al-Degs [25]. This observation would indicate that the amount of zinc precipitation is so low with respect to the amount of mineral sample that the intensity of the corresponding bands is not high enough to be detected. It is reported that the sorption of zinc on pure calcite produces hydroxyl and carbonate complexes of zinc within the crystal structure of calcite [26], giving another probable explanation.

Absorption bands at 998 and 669 cm^{-1} in line *a* come from the vibration of Fe–OH group which can be assigned to the component of goethite in the adsorbent by XRD patterns. This mineral has been reported active for Zn(II) adsorption [27,28]. The presence of Fe–OH group can also be identified in lines *b* and *d*. The band at 669 cm^{-1} in CAL disappears after treated with acid, indicating the dissolution of ferrous oxide. The intensity of this band also declines in Zn(II) loaded CAL, suggesting the complexation of Zn(II) with Fe–OH groups in the form of:

$$Zn^{2+} + 2[\text{Fe–OH}] \rightarrow [\text{Fe–O–Zn–O–Fe}] + 2H^+ \quad (14)$$

The bands at 668 and 2360 cm^{-1} correspond to atmospheric carbon dioxide. These peaks are not observed at line *b* for the sample was obtained by rinsing in $ZnSO_4$ solution for 24 h. Thus the originally adsorbed CO_2 might be dissolved into water and the pores would be filled by water or Zn(II). For other samples, CO_2 may be adsorbed from the air onto the adsorbents during the storage period. It is observed that the IR bands of CO_2 on the calcinated sorbent are stronger than those of the crude loess, indicating the improved surface and micropore structures beneficial to higher sorption capacity which is consistent with the morphology of the sorbent shown in TEM photos.

The absorption band at 2920 cm^{-1} can be related to C–H group. This pattern occurs in CL, CAL and ATCAL, except in Zn(II) loaded CAL. Associated with the presence of OH and CH groups, organics is identified as a common constituent in natural CL and is considered responsible for the high adsorption capacity of CL. The C–H group in CAL may be ascribed to the contamination of the sorbent by carboxyl gases in air.

The analysis of isotherms indicates that the sorption of Zn(II) on CAL is multilayered (due to Freundlich model) and in form of ion exchange (due to D–R model). The former is consistent with the morphology of the soil particles by TEM photos as well as the speculations that the adsorption involves diffusion into the micropores of soil particles by intraparticle diffusion kinetics. The latter is verified by the decreased calcite content after adsorbed with Zn(II) in XRD and FT-IR patterns as well as the decreased entropy changes.

A chemisorption of Zn(II) on ATCAL was suggested by the mean free energy of adsorption which was predicted as −23.224 kJ mol^{-1} by D–R model. Because the calcite and surface OH group have been largely removed from the sorbent by acid washing, the ion exchange type adsorption cannot happen in this situation. After calcination, the kaolinite component is partly transformed into montmorillonite. The expanded spaces between the mineral slices will be the preferential sorption sites for Zn(II) and thus make the pore-filling physisorption possible. The free energy of D–R model is an average value; therefore, the coexistence of the above mechanisms may not be controversial.

Table 7
Adsorption capacities of Zn(II) on different natural adsorbents

Reported adsorbents	Zn(II) adsorption capacity (mg g^{-1})	References
Activated carbon	1.6	[29]
Bigadic zeolite	3	[30]
Gordes zeolite	6	[30]
Natural Bentonite	24	[17]
Natural Jordanian soil	184	[31]
CAL	113.6	This study
CL	216.0	This study

The Zn(II) adsorption capacities of several reported natural sorbents are listed in Table 7 for comparison [19,30–32]. The activated carbon, Bigadic zeolite and Gordes zeolite were reported with 1.6, 3 and 6 mg g^{-1} Zn(II) adsorption capacity, respectively. The natural bentonite was reported to have somewhat higher sorption capacity at 24 mg g^{-1}. These materials are all single components with low impurities. Although the porosity is high in both activated carbon and zeolite, the low Zn(II) sorption capacity reveals the failure of diffusion into the inner micro- or mesopores. On the contrary, natural soil containing complex mineral constituents have high Zn(II) adsorption capacity (184 mg g^{-1} for natural Jordanian soil). Similarly, the Chinese loess also contains complex components and possesses high sorption capacity, indicating that the chemical reactions existed wherein must play important roles in this process. The high efficiency of Zn(II) removal by CAL can be confirmed in this manner.

3.9. Treatment of byproduct

Acid wash with HCl at pH 2.0 can eliminate about 99.95% of the adsorbed Zn(II) on CAL and about 99.50% on ATCAL. The residual concentrations of Zn(II) on the treated byproducts were 51.5 and 77.4 mg kg^{-1} for CAL and ATCAL, respectively, both less than the maximum acceptable concentration of Zn(II) for Grade 1 soil following the Chinese Environmental Quality Standard for Soils [29]. For ATCAL, the sorption capacity can still reach 15.9 mg g^{-1}, about one-sixth of that of CAL. Since these residual minerals are stable and will not be decomposed in common conditions, it is likely that the sorbent can be recycled by acid wash. The new sorbent developed by calcinations of crude loess is accessible for industrial utilization.

4. Conclusions

(1) Calcinations of crude loess proved to be effective in improving the separation efficiency for slurries and to increase the particle sizes of the sorbent.
(2) The Zn(II) adsorption amount on CAL increases steadily with increasing equilibrium pH and with decreasing slurry concentration and temperatures.
(3) The sorption capacities of different sorbents are sequenced as CL > CA L > DCL > ATCAL. The adsorption on CAL is multilayered, exothermic and spontaneous and the isotherm follows the Freundlich model. The kinetic study shows that the test data fits the pseudo-second order kinetics well.
(4) The Zn(II) adsorption on CAL is of the ion exchange type chemisorption with calcite and goethite due to FT-IR and XRD patterns as well as the predicted mean free energies (−11.58 to −9.28 kJ mol^{-1}).
(5) The byproduct of adsorption can be purified and refreshed by 0.01 M HCl solution. The adsorption capacity of Zn(II) on ATCAL is determined as 15.89 mg g^{-1} with preferential chemisorption between the mineral slices.

Acknowledgments

The authors would like to express their sincere gratitude to the Key Project of National Natural Science Foundation of China (NSFC) (Grant 50538080) and National Science Fund for Distinguished Young Scholars (Grant 50425825) for the financial support to this study. The helps from Professor D.G. Fredlund in proof checking of this paper and the comments from two anonymous reviewers are also appreciated.

References

[1] J.A. Grout, C.D. Levings, Effects of acid mine drainage from an abandoned copper mine, Britannia Mines, Howe Sound, British Columbia, Canada, on transplanted blue mussels (*Mytilus edulis*), Mar. Environ. Res. 51 (2001) 265–288.
[2] C. Lin, Y. Wu, W. Lu, A. Chen, Y. Liu, Water chemistry and ecotoxicity of an acid mine drainage-affected stream in subtropical China during a major flood event, J. Hazard. Mater. 142 (2007) 199–207.
[3] R. Gieré, N.V. Sidenko, E.V. Lazareva, The role of secondary minerals in controlling the migration of arsenic and metals from high-sulfide wastes (Berikul gold mine, Siberia), Appl. Geochem. 18 (2003) 1347–1359.
[4] M.T. Alvarez, C. Crespo, B. Mattiasson, Precipitation of Zn(II), Cu(II) and Pb(II) at bench-scale using biogenic hydrogen sulfide from the utilization of volatile fatty acids, Chemosphere 66 (2007) 1677–1683.
[5] M. Lee, I.S. Paik, I. Kim, H. Kang, S. Lee, Remediation of heavy metal contaminated groundwater originated from abandoned mine using lime and calcium carbonate, J. Hazard. Mater. 144 (2007) 208–214.
[6] E. Pehlivan, T. Altun, The study of various parameters affecting the ion exchange of Cu^{2+}, Zn^{2+}, Ni^{2+}, Cd^{2+}, and Pb^{2+} from aqueous solution on Dowex 50W synthetic resin, J. Hazard. Mater. 134 (2006) 149–156.
[7] M.F. Sawalha, J.R. Peralta-Videa, J. Romero-González, M. Duarte-Gardea, J.L. Gardea-Torresdey, Thermodynamic and isotherm studies of the biosorption of Cu(II), Pb(II), and Zn(II) by leaves of saltbush (*Atriplex canescens*), J. Chem. Therm. 39 (2007) 488–492.
[8] N. Meunier, J. Laroulandie, J.F. Blais, R.D. Tyagi, Cocoa shells for heavy metal removal from acidic solutions, Bio. Tech. 90 (2003) 255–263.
[9] M.T.K. Tsui, K.C. Cheung, N.F.Y. Tam, M.H. Wong, A comparative study on metal sorption by brown seaweed, Chemosphere 65 (2006) 51–57.
[10] J.O. Agbenin, L.A. Olojo, Competitive adsorption of copper and zinc by a Bt horizon of a savanna Alfisol as affected by pH and selective removal of hydrous oxides and organic matter, Geoderma 119 (2004) 85–95.
[11] K. Bellir, M. Bencheikh-Lehocine, A.H. Meniai, N. Gherbi, Study of the retention of heavy metals by natural material used as liners in landfills, Desal 185 (2005) 111–119.
[12] D. Craw, Potential anthropogenic mobilisation of mercury and arsenic from soils on mineralised rocks, Northland, New Zealand, J. Environ. Manage. 74 (2005) 283–292.
[13] A. García-Sánchez, E. Álvarez-Ayuso, Sorption of Zn, Cd and Cr on calcite. Application to purification of industrial wastewaters, Miner. Eng. 15 (2002) 539–547.
[14] K. Cave, F.I. Talens-Alesson, Comparative effect of Mn(II) and Fe(III) as activators and inhibitors of the adsorption of other heavy metals on calcite, Coll. Surf. A: Physicochem. Eng. Asp. 268 (2005) 19–23.
[15] A.M. Assallay, C.D.F. Rogers, I.J. Smalley, I.F. Jefferson, Silt: 2–62 μm, 9–4φ, Earth-Sci. Rev. 45 (1998) 61–88.
[16] S. Sudou, Clay Minerals (S.H. Yan, Trans.), Geology Press, Beijing, 1981 (in Chinese).
[17] V.E. Kalm, N.W. Rutter, C.D. Rokosh, Clay minerals and their paleoenvironmental interpretation in the Baoji loess section, Southern Loess Plateau, China, Catena 27 (1996) 49–61.
[18] D.H. Eom, J.G. Park, E.S. Lee, Effect of organic acids in copper chemical mechanical planarization slurry on slurry stability and particle contamination on copper surfaces, Jpn. J. Appl. Phys. 41 (2002) 1305–1310.
[19] A. Kaya, A.H. Oren, Adsorption of zinc from aqueous solutions to bentonite, J. Hazard. Mater. 125 (2005) 183–189.
[20] D.D. Do, Adsorption Analysis: Equilibrium and Kinetics, Imperial College Press, London, 1998.
[21] Y.S. Ho, G. McKay, A comparison of chemisorption kinetic models applied to pollutant removal on various sorbents, Trans. Inst. Chem. Eng. 76B (1998) 332–340.
[22] N. Ünlü, M. Ersoz, Adsorption characteristics of heavy metal ions onto a low cost biopolymeric sorbent from aqueous solutions, J. Hazard. Mater. 13 (2006) 272–280.
[23] C.H. Giles, D. Smith, A. Huitson, A general treatment and classification of the solute adsorption isotherm: I. Theoretical, J. Colloid Interf. Sci. 47 (1974) 755–765.
[24] F. Berna, R. Shahack-Gross, A. Behar, Sediments exposed to high temperatures: reconstructing pyrotechnological processes in Late Bronze and Iron Age Strata at Tel Dor (Israel), J. Archaeol. Sci. 34 (2007) 358–373.

[25] Y.S. Al-Degs, M.I. El-Barghouthi, A.A. Issa, M.A. Khraisheh, G.M. Walker, Sorption of Zn(II), Pb(II), and Co(II) using natural sorbents: equilibrium and kinetic studies, Water Res. 40 (2006) 2645–2658.
[26] E.J. Elzinga, R.J. Reeder, X-ray absorption spectroscopy study of Cu^{2+} and Zn^{2+} adsorption complexes at the calcite surface: implications for site-specific metal incorporation preferences during calcite crystal growth, Geochim. Cosmochim. Acta 66 (2002) 3943–3954.
[27] P. Trivedi, L. Axe, T.A. Tyson, An analysis of zinc sorption to amorphous versus crystalline iron oxides using XAS, J. Colloid Interf. Sci. 244 (2001) 230–238.
[28] M. Nachtegaal, D.L. Sparks, Effect of iron oxide coatings on zinc sorption mechanisms at the clay-mineral/water interface, J. Colloid Interf. Sci. 276 (2004) 13–23.
[29] GB 15618-1995, Chinese Environmental Quality Standard for Soils, Standard Press of China, Beijing, 1995.
[30] M.M. Gómez-Tamayo, A. Macías-García, M.A.D. Díez, E.M. Cuerda-Correa, Adsorption of Zn (II) in aqueous solution by activated carbons prepared from evergreen oak (*Quercus rotundifolia L.*), J. Hazard. Mater. 153 (2008) 28–36.
[31] A.H. Ören, A. Kaya, Factors affecting adsorption characteristics of Zn^{2+} on two natural zeolites, J. Hazard. Mater. 131 (2006) 59–65.
[32] M.A.M. Khraisheh, Y.S. Al-degs, W.A.M. Mcminn, Remediation of wastewater containing heavy metals using raw and modified diatomite, Chem. Eng. J. 99 (2004) 177–184.